JOURNAL OF MATERIALS SCIENCE 30 (1995) 4703–4709

Microstructure of aluminium–alumina–silica particulate composites obtained by reactive sintering

S. MINTZER, M. IPOHORSKI, S. BERMÚDEZ
Departamento Technología de Materiales, Gerencia Desarrollo, Comisión Nacional de Energía Atómica Av.del Libertador 8250, 1429 Buenos Aires, Argentina

In the present work aluminium–alumina–silica particulate metal matrix composites (PMMCs) with different percentages of ceramic were obtained by liquid phase reactive sintering of pure aluminium and a proportion of silica powder ranging from 5 up to 20 vol %. Sintering was carried out at 893 K for 24 h in vacuum. A relatively long sintering time was selected in order to approach the chemical equilibrium state. The microstructure of the composites was studied using optical metallography, X-ray diffraction, scanning electron microscopy (SEM) and electron probe microanalysis (EPMA). At the sintering conditions the study indicates the presence of α-alumina, silica coesite (a high density polymorphic transformation of silica), a solid solution of silicon in aluminium, and pure silicon platelets.

Sintered properties such as dimensional changes, hardness, and open and total porosity, were measured. Porosity increases with the particle content. Maximum shrinkage was obtained at ≈ 10 vol % ceramic content. Brinell hardness increases from 24 BHN for sintered pure Al up to 46 BHN for the 20 vol % ceramic specimens.

Initial results indicate that, by an appropriate selection of sintering temperature and hold time, composites with different proportions of the above mentioned phases and thus with different mechanical properties could be obtained. Liquid phase reactive sintering is shown to be an alternative and simple method for the obtention of some PMMCs.

1. Introduction

In the last ten years there has been increasing interest in the development of metal matrix composites (MMCs) reinforced with ceramics: either fibres, whiskers or particles. Composite materials with good wear resistance, improved strength and stiffness, or thermal and electrical properties intermediate between those corresponding to the metal and the ceramic could thus be obtained [1]. Particularly a great interest has been shown recently in the potential applications of ceramic PMMCs due to the low cost of fabrication and the fact that they can be mechanically worked like conventional wrought alloys. An additional advantage is the isotropy of their physical and mechanical properties.

The obtention of PMMCs involves the adequate combination of the metal or alloy with the reinforcing phase followed by an appropriate fabrication method. Several processing techniques have been developed in order to optimize the structure and properties of PMMCs. The fabrication techniques can be classified according to the state of the metal matrix during processing, in the following categories [2]:

1. *Liquid phase processes.* In this group the ceramic phase is incorporated in a molten metallic matrix followed by an adequate mixing and casting, e.g. vortex technique [3], squeeze casting [4, 5], XD™ process developed by Martin Marietta Laboratories [6].

2. *Solid phase processes.* Rapidly solidified metallic powders are sieved and blended with the ceramic particulate reinforcement, then pressed and sintered, usually combined with some hot working operation (hot rolling, pressing or extrusion) in order to improve the mechanical properties of the composites. With some differences, this technology has been developed by several commercial manufacturers (Alcoa, Ceracon Inc., DWA Composites Inc.).

3. *Two Phase Processes.* Solid and liquid phases coexist during the fabrication process, e.g. compocasting [7], Osprey deposition [8], variable co-deposition of multiphase materials [9].

The above mentioned methods have their specific advantages and disadvantages, see for instance [2]. However, a survey of the open literature shows that the use of reactive sintering, especially with a liquid phase present, has not apparently been exploited as an alternative fabrication route for the obtention of ceramic PMMCs. This approach can be used whenever a chemical reaction occurs between a reactive metal matrix (Al, Ti, Mg, Ni) and the ceramic particles at the sintering temperature. This process falls in group 3 of the above mentioned classification. Although fibre degradation by chemical reaction can occur in fibre-reinforced composites, this is not a problem with the particles in PMMCs. A review of previous work on reactive sintering indicates that this possibility is still

0022–2461

in the developmental stage, although there were some efforts to obtain ceramics [10, 11], intermetallic compounds [12], and Ti compounds (e.g. TiC, TiB_2) by self-propagating synthesis [13].

The present study considers reactive sintering applied to aluminium and silica powders as an alternative and simple fabrication route for the *in-situ* obtention of aluminium–alumina–silica PMMCs. Al and SiO_2 powders were selected as base materials as they have several attractive characteristics such as low cost, availability, and low sintering temperatures at which composites can be obtained. Silica and alumina are interesting reinforcing materials due to their high hardness and good abrasion resistance. Powder mixtures with different initial percentages of silica particles were considered: 5, 10, 15 and 20 vol %. As a reference material, pure Al powder was sintered with the same vol percentages of alumina in similar conditions.

The primary purpose of the present work was to investigate the effects of the chemical reactions occurring during sintering on the microstructure of the composites, and the changes which take place with particle content. In order to reach a chemical equilibrium state a relatively long sintering time was considered (24 h at 893 K) but shorter times and/or other temperatures may be used for the obtention of PMMCs [14]. The study of the influence of sintering parameters on the thermomechanical properties of the $Al–Al_2O_3–SiO_2$ composites is underway and will be the subject of a future publication [14].

2. Materials and experimental procedure

Starting materials for the reactive sintering experiments were atomized Al powder of commercial purity (main impurities: 0.2% Fe, 0.05% Cu, 0.02% Si) and silica powder (major impurities: 0.3% Al_2O_3, 0.1% Fe_2O_3, 0.1% CaO). Scanning electron micrographs (SEM) of the sieved Al powder showed particles to be elongated in shape (Fig. 1(a)), with an average length of 100 μm and average diameter 50 μm. The non-spherical shape of the Al powder may be an indication that the powder was atomized in air with a relatively thick surface oxide layer (the oxide tends to reduce the surface tension of the droplets). Sieved (450 mesh) silica powder, Fig. 1(b), was composed of irregular particles with an average size of 20 μm. Some agglomerates of the silica particles were also visible in the SEM micrographs.

In order to eliminate possible volatile contaminants, silica powder was heat treated at 1023 K for 1 h. Al and SiO_2 powders were afterwards mixed by conventional techniques using a Y-type mixer in the following proportions: 5, 10, 15 and 20 vol % silica. The blends thus obtained were then cold-compacted in a double action matrix in a hydraulic press. Sintering was performed under dynamical vacuum (≈ 0.013 Pa) for 24 h at 893 ± 3 K. In all cases the resulting cylindrical pellets were ≈ 13.1 mm in diameter and about 18 mm in height. As reference materials, pure Al and Al–alumina mixtures with the same

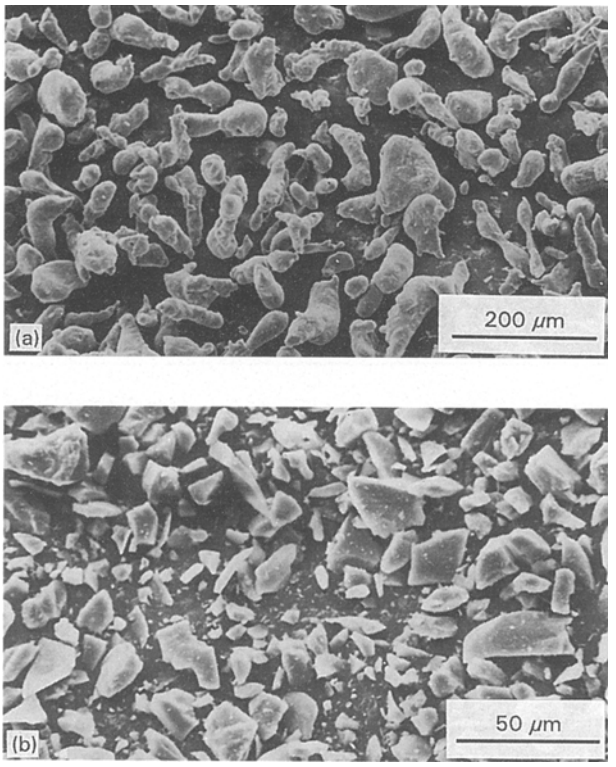

Figure 1 (a) SEM of the aluminium powder. (b) SEM of the α-silica powder.

volume percentages of ceramic were processed and sintered in similar conditions.

Metallographic samples were afterwards prepared by standard procedures. Optical metallography of either polished and/or etched (Keller's etch) specimens provided direct insight about the distribution of particles, phases and pores present after reactive sintering. Qualitative and quantitative electron probe microanalysis (EPMA) was used for composition determination of phases and analysis of the particle–matrix interface. Open and total porosity determinations were performed by impregnation using standard hydrostatic methods. Mechanical testings consisted of Brinell hardness determinations using a load of 5 kg and a 1 mm diameter ball. Relative dimensional changes (radial) before and after sintering were also measured. In both cases a minimum of three samples was tested for each particle content and the average value is reported.

3. Results

Typical microstructures of PMMCs are shown in the optical micrographs of Fig. 2(a), (b) and (c) corresponding to samples of Al–5 vol % SiO_2, Al–10 vol % SiO_2 and Al–20 vol % SiO_2 respectively (from now onwards percentages are always understood as initial volume percent of silica in the mixtures and will be referred to as ceramic content). Together with the metal matrix and the ceramic particles another phase consisting of fine platelets appears. Length and thickness, as well as the amount of platelets, increase with the initial silica content of the specimens. In the samples containing 5 and 10 vol % ceramic, the platelets are preferentially arranged around the particles and

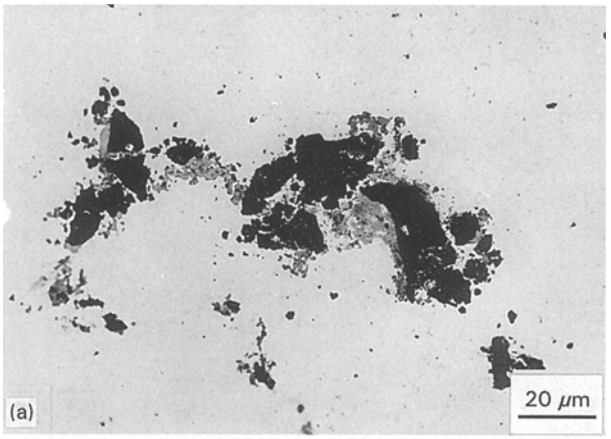

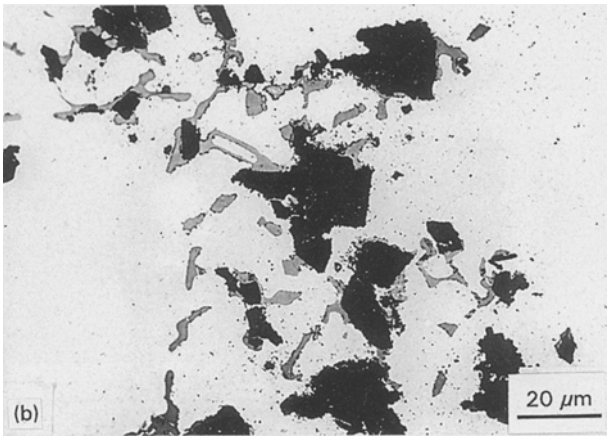

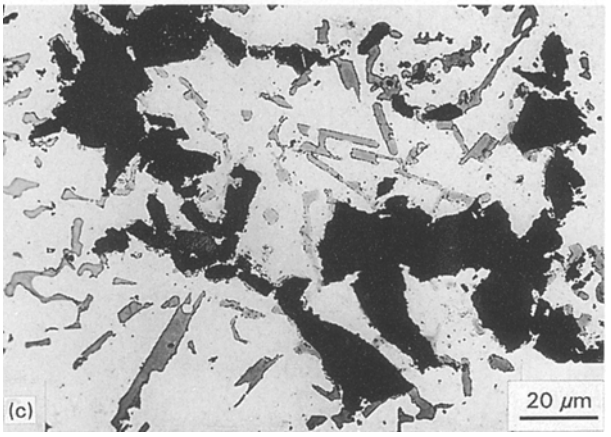

Figure 2 Typical optical micrographs showing the changes of the PMMCs microstructure with ceramic content after reactive sintering of aluminium and silica, for (a) 5 vol % ceramic; (b) 10 vol % ceramic; (c) 20 vol % ceramic.

the grain boundaries of the metallic matrix. An inspection at higher magnifications shows an increase in the amount of these platelets around the smaller ceramic particles of the distribution (higher surface to volume ratio). In the specimens with higher initial silica content (15 and 20 vol % ceramic) the platelets are more uniformly distributed between ceramic particles (Fig. 2(c)). Our observations also show isolated pores, usually located near previous agglomerates of small silica particles or near the clusters of the larger ones.

Electron microprobe (EPMA) micrographs (Fig. 3(a)), show that bonding exists between ceramic particles and matrix, except in places where the particles are clustered. Quantitative analysis performed by EPMA in the sintered samples, showed that the metal matrix consists of a Si solid solution in Al, with the following average concentration of Si: 1.3 at % for Al–5 vol % ceramic, 1.4 at % for Al–10 vol % ceramic, and 1.5 at % for the Al–15 vol % and 20 vol % ceramic specimens. EPMA also showed the platelets to be composed of pure Si. Fig. 3(b) corresponds to the X-ray mapping of Al in the Al–10 vol % ceramic specimen. Large white regions correspond to the Al matrix containing small percentages of Si (solid solution of Si in Al). Fig. 3(c) shows the X-ray mapping of Si in the same region. Bright zones indicate Si being present in the platelets (upper left) and in the metal–ceramic interphases. A further inspection of the specimens by EPMA showed that for the sintering time considered, ceramic particles were mainly composed of alumina. A comparison of Fig. 3(a) and (c) shows the ceramic particle–metal matrix boundary to be mostly composed of pure Si. The strength of a MMC is achieved by transfer of load from the reinforcing phase through the strong interface between the two materials. The reaction leading to the formation of a Si surface layer provides a strong coherent bond between the metal matrix and the ceramic particles.

On the other hand, X-ray diffraction determinations (Fig. 4) showed the existence of the following phases: Al (peaks A), Si (peaks S), silica–coesite (peaks B) and alumina (peaks C). The heights of the diffraction peaks of Si, SiO_2 and Al_2O_3 increase, as the initial silica content is increased, in comparison with the peaks of Al. It is interesting to note the presence of silica–coesite which is a polymorphic form of silica that appears only at high pressures.

Fig. 5 shows the variation of total and closed porosity (difference between total and open porosity) as a function of the ceramic content. Both types of porosity increase with the ceramic content. Fig. 5 also shows that the increase of total porosity is due mainly to the increase of the open porosity.

The relative dimensional changes of the samples are plotted in Fig. 6. The radial dimensions of the compacts, normal to the compacting direction, decrease after sintering, except for the 20 vol % ceramic content. Maximum shrinkage appears at about 10 vol % ceramic. It has also been observed that for higher particle content there is a slight tendency for swelling.

Fig. 7 shows the variation of Brinell hardness number (BHN) with the volume percentage of ceramic. The sintered hardness increases, the rate of increase being higher up to ≈ 10 vol % ceramic. Also, for each particle content, the dispersion of the hardness data in the samples increases with the ceramic content.

Finally, it is interesting to note the results obtained mixing pure Al powder directly with Al_2O_3 particles (5, 10, 15 and 20 vol %) compacted and sintered under similar conditions. In these cases chemical reactions are not possible and the sintered samples (solid state sintering) had poor bonding characteristics between metal and ceramic particles and a porous material results.

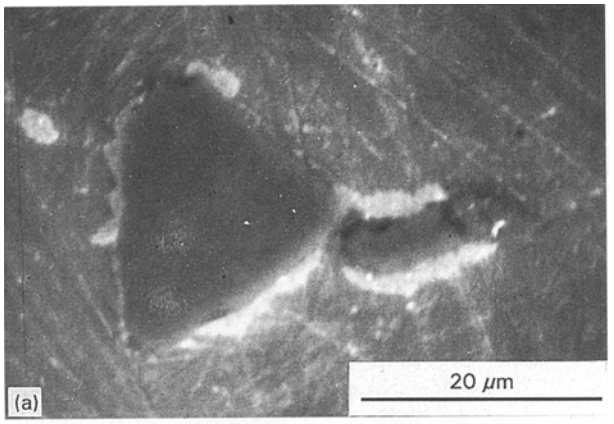

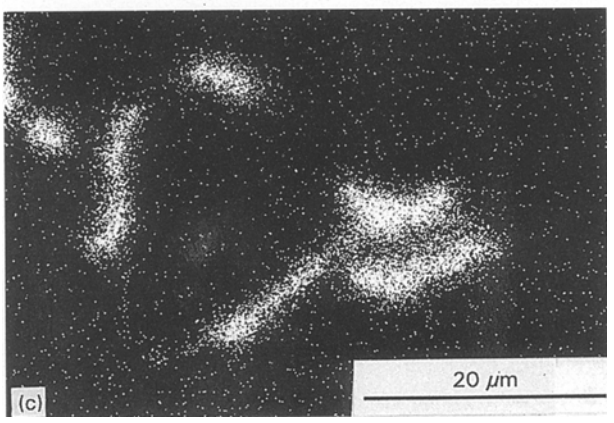

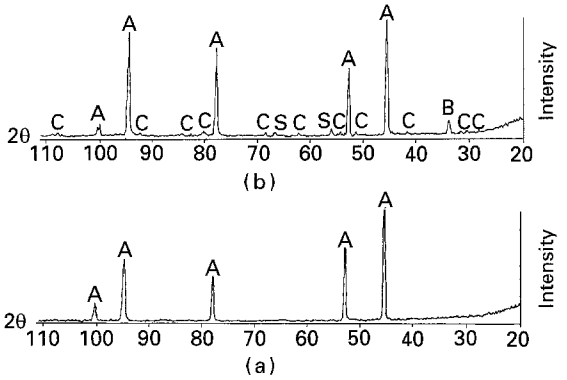

Figure 4 X-ray diffraction pattern of (a) sintered aluminium, and (b) composite with 10 vol % ceramic. Line identification: Al (peaks A), Si (peaks S), silica coeasite (peaks B), and alumina (peaks C).

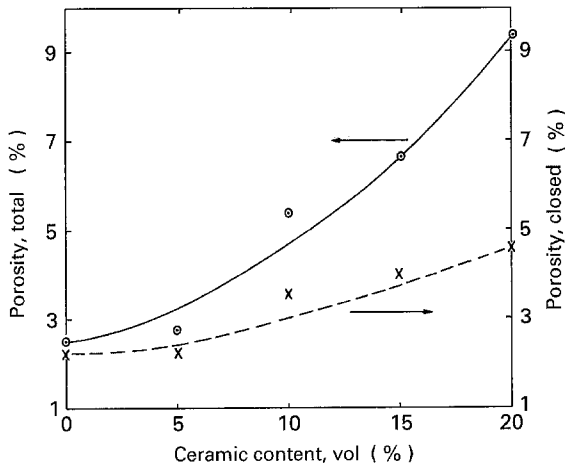

Figure 5 Effect of ceramic content on the total and closed porosity of the composites.

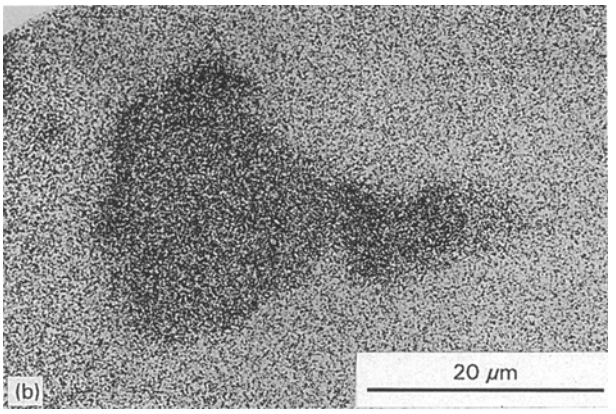

Figure 3 SEM (a), and X-ray images of aluminium (b) and silicon (c), corresponding to the composite with 10 vol% ceramic after reactive sintering (893 K, 24 h).

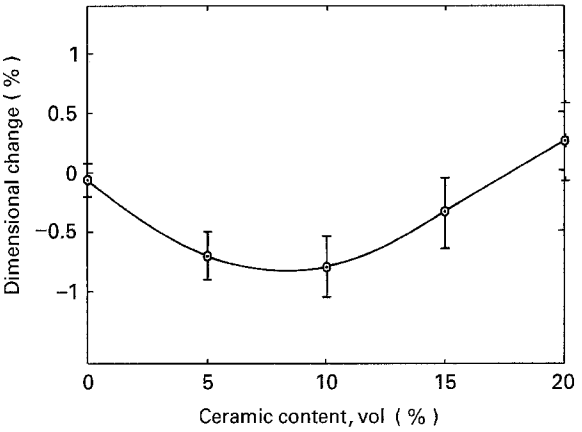

Figure 6 Relative dimensional changes as a function of ceramic content.

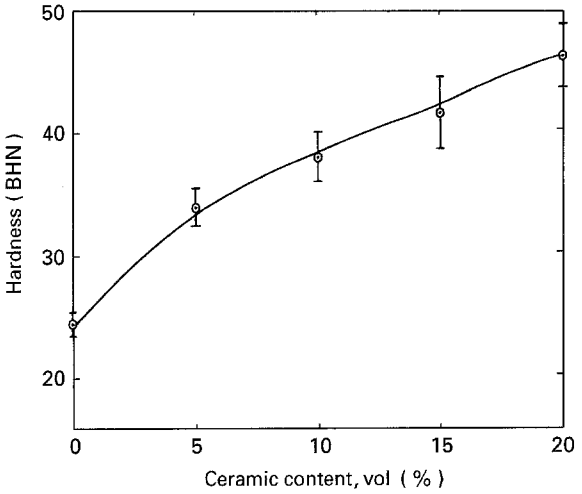

Figure 7 Variation of hardness (Brinell) with the ceramic content of the composites.

4. Discussion

4.1. Sintered microstructure

The presence of the above mentioned phases in aluminium samples containing initially only silica can be explained in terms of the high affinity which presents aluminium for oxygen. At 893 K the standard free energy of the formation of aluminium oxide

($\Delta G(Al_2O_3) = -220\,kcal\,mol^{-1}$) is more negative than that of silica ($\Delta G(SiO_2) = -170\,kcal\,mol^{-1}$) [15]; thus aluminium will have a reducing effect on silica. The chemical reaction

$$4Al\,(s) + 3SiO_2\,(s) \rightarrow 3Si\,(s) + 2Al_2O_3\,(s) \quad (1)$$

is thermodynamically favoured since it is accompanied by a net decrease ($-50\,kcal\,mol^{-1}$) of free energy.

The kinetics of the reaction between quartz (amorphous) and aluminium has been studied by Standage and Gani [16] introducing quartz rods in the liquid metal. They found that the reaction follows an Arrhenius type temperature dependence, and the width of the transformed zone increases linearly with time after a certain incubation period. The Arrhenius temperature dependence was also found by Prabriputaloong and Piggot [17]. On the other hand, the Al–Si phase diagram [18] presents an eutectic point of composition Al–12.2 at % Si at 850 K. In the current literature, no intermetallic compounds, either stable or metastable, were reported to exist in this system.

According to the previous considerations, and taking into account the metallographic, EPMA and X-ray determinations, when the compacts containing initially only Al with 5, 10, 15 and 20 vol % silica are sintered at 893 K, a series of transformations take place. Fig. 8 shows a schematic diagram of the reactive sintering process in Al–silica as envisioned from our observations. The sintering process of the green pellets starts with β-silica particles in a pure Al matrix (Fig. 8(a) time $t = t_0$), because at 846 K the following

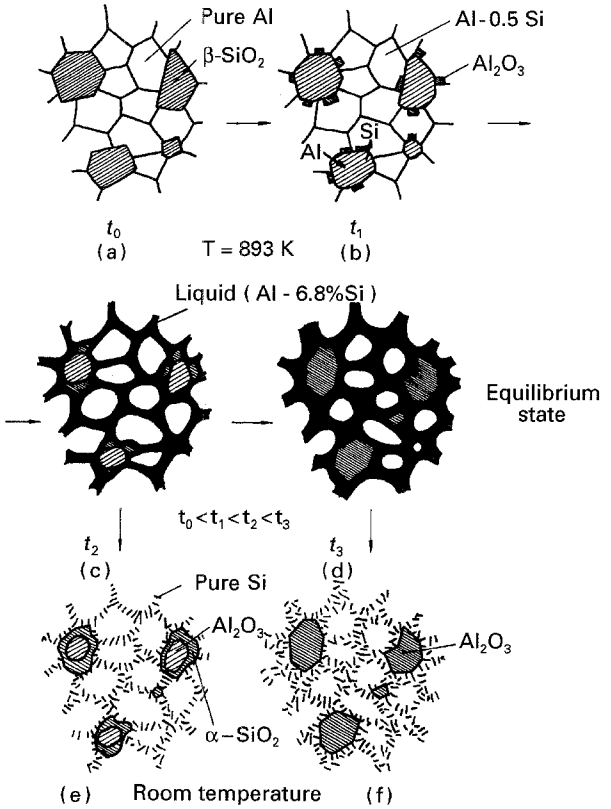

Figure 8 Schematic diagrams illustrating the progress of reactive sintering as a function of hold time (t) at a given temperature: (a) t_0; (b) t_1; (c) t_2; (e), short sintering time; (a) t_0; (b) t_1, (c) t_2, (d) t_3, long sintering time, (f) final state in chemical equilibrium.

displacive transformation takes place: α-SiO_2 (tetragonal) → β-SiO_2(hexagonal). The thin alumina layer which usually covers Al particles cracks down in the metal–silica and metal–metal contact regions after cold compacting. In these regions, at the sintering temperature, Al reacts with β-silica particles according to Equation 1, and Si diffuses to the metallic matrix (Fig. 8(b) time $t = t_1$). The process in its early stages is a solid state sintering in those regions. As the reaction proceeds, silicon enters in solid solution up to a maximum of 0.8 at %. On the other hand, since Al does not dissolve oxygen, an alumina layer gradually builds up over the ceramic particles (Fig. 8(c) time $t = t_2$). A liquid phase of composition Al–6.8 at % Si appears according to the phase diagram. The amount of liquid increases as β-silica is being dissolved.

On cooling to room temperature, the sintering process is interrupted (Fig. 8(e)) and the hypo-eutectic liquid solidifies giving rise to Al pro-eutectic crystals and a binary eutectic of composition Al–12.2 at % Si. This acicular eutectic contains the Si platelets observed by optical microscopy (Fig. 2) and EPMA (Fig. 3).

The process described here corresponds to a persistent liquid phase reactive sintering. Besides the initial phases (Al, SiO_2) new phases are formed after the sintering: Al_2O_3, solid solution of Si in Al, and the liquid phase which persists during the whole sintering process. For each initial particle content (silica) by varying sintering temperature and/or time it is possible to obtain specimens with different proportions of silica, alumina and silicon.

Due to the presence of the liquid phase, densification occurs through the capillary forces exerted by the liquid on the solid particles. The observed tendency towards shrinkage (Fig. 6) is a direct consequence of such densification process.

According to the kinetics of the reaction Al–SiO_2 (Equation 1) the amount of densification obtained in the rearrangement stage has a strong dependence with temperature and sintering time for a given particle content. Concurrently with the rearrangement stage, densification is also produced by the solution–reprecipitation process [19]. In this process, which is characteristic of many systems sintering with a liquid phase present, solubility of the metal matrix grains is inversely proportional to the grain size. A concentration gradient is thus built up between the grains due to the difference in solubilities. A net transport of material from the smaller grains towards the larger ones occurs by diffusion in the liquid [19]. The size of the larger grains thus increases progressively.

Fig. 9 shows a micrograph of a liquid phase sintered microstructure with grain coarsening in an Al–5 vol % ceramic content specimen for the relatively long sintering time considered. The solid solution grains (mean diameter 134 μm) are larger than the original Al powder particle size. Further growth of the grains is restricted by the presence of the ceramic particles.

If the sintering process were to be continued for a longer time (Fig. 8(d) time $t_3 > t_2$) chemical equilibrium would be reached with a total transformation of β-silica into alumina particles. The EPMA

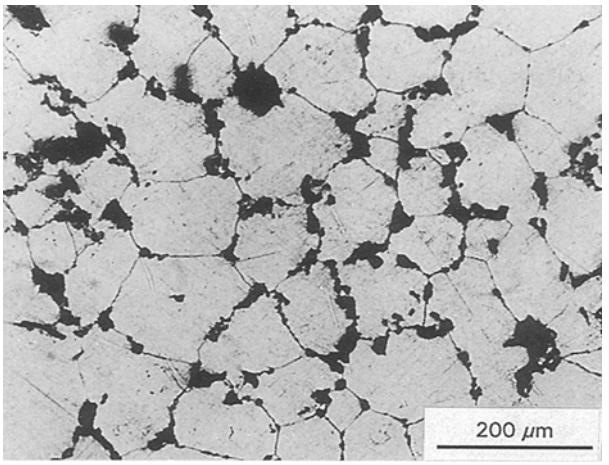

Figure 9 Optical micrograph showing grain boundary pinning by ceramic particles which occurs after long sintering times (893 K, 24 h).

determinations have shown that, after sintering at 893 K for 24 h, the majority of the ceramic particles present corresponds to alumina. According to the X-ray diffraction results (Fig. 4) the remaining quartz particles, located most probably in the larger ceramic particles, correspond to silica–coesite (monoclinic). This polymorphic transformation [20] gives rise to a very dense variety of quartz, since the specific gravity of coesite ($\delta = 3.01\,g\,cm^{-3}$) is appreciably larger than that corresponding to α-silica ($\delta = 2.52\,g\,cm^{-3}$). Investigating the structure of silica, Coes [20] found that coesite forms only at high pressures. The presence of coesite in our composites could be accounted for by the high thermal differential contraction stresses at the metal–ceramic interphase originated in the different thermal expansion coefficients of the metal matrix and quartz. These stresses produce a many orders of magnitude increase of the dislocation density around the ceramic particles. In fact, Arsenault and colleagues [1] have observed in transmission electron micrographs of Al alloys containing silicon carbide particles that dislocation densities as high as $10^{13}\,cm^{-2}$ exist in the metal–ceramic interphase as a consequence of the thermal stresses.

4.2. Porosity

The observed increase of porosity with particle content of the final composites (Fig. 4) can be attributed to different factors, First, as mentioned in Section 3, some agglomerates exist already in the starting silica powder as a result of Van der Waals attractive forces. This is common to many commercial ceramic powders. In practice the agglomerates are not dispersed during compaction of the green pellets due to the strong bonding between particles. Some clustering of originally isolated particles could also occur during blending as a consequence of electrostatic forces developed by friction between the powder particles. In both cases the reactive sintering process is restricted and does not proceed fully in the agglomerates or clusters. Voids can be formed instead in such places.

A second factor should be considered in order to account for the increase of porosity. The thin film of aluminium oxide of ≈5 nm thickness formed during the atomization of the Al [21, 22] contains water vapour, aluminium hydroxide and oxygen retained by physical adsorption. During heating at the sintering temperature several chemical reactions can take place, for instance [21]

$$\begin{aligned} 2Al + 3H_2O &\rightarrow Al_2O_3 + 3H_2 \\ Al_2O_3 \cdot 3H_2O &\rightarrow Al_2O_3 + 3H_2O \\ 2Al + 6H_2O &\rightarrow Al_2O_3 \cdot 3H_2O + 3H_2 \end{aligned} \quad (2)$$

In all cases a very stable layer of alumina is formed. The presence of such films can inhibit the reactive sintering process between aluminium and silica especially in the lower density regions of the compacts. As a consequence of die pressing, a gradient of density is always present in the compacts. Density is lower in the vicinity of lateral free surfaces, thus contributing to the observed increase of open porosity (Fig. 5).

It can also be seen from Fig. 5 that, as far as porosity is concerned, there is an optimum amount of initial silica particles (≈10 vol %) which could be incorporated into the aluminium matrix. For composites with higher ceramic content, closure of the porosity could be done if the specimens are either hot-rolled, -forged, -extruded or -pressed, or by a combination of cold repressing and resintering.

4.3. Hardness

Compared to Al, the observed increase in hardness with the ceramic particle content (Fig. 7) can be explained by the combined roles of solid solution hardening, ceramic particles, precipitation hardening (Si platelets) and porosity. For a particle content up to ≈10 vol % the sharp increase in the hardness of the composites can be attributed to the first three mechanisms mentioned above, and to a low porosity. For higher ceramic contents, the influence of porosity becomes dominant. A slight additional increase is obtained, up to 46 BHN for 20 vol % ceramic content, which is comparable to the value of some wrought duralumin alloys.

The porosity distribution and density are also responsible for the higher dispersion observed in the hardness of similar ceramic content specimens as the ceramic content increases.

5. Conclusions

1. Aluminium–alumina–silica particulate metal matrix composites (PMMCs) with different volume percentages of ceramic (5, 10, 15 and 20 vol %) were obtained by liquid phase reactive sintering of pure aluminium and silica powder.

2. The study of the microstructure of the composites using optical microscopy, electron probe microanalysis (EPMA) and X-ray diffraction techniques, shows that after reactive sintering of Al and SiO_2 at 893 K in vacuum for 24 h, the specimens contain α-alumina, silica–coesite, a solid solution of Si in Al, and pure Si platelets. The study also indicates that at the sintering

conditions considered most of the initial silica has been transformed into alumina, and that the amount of Si platelets as well as Si in solid solution increase with the ceramic content. The reaction leading to the formation of a Si interface between ceramic particles and the Al matrix also provides a strong coherent bond between both materials.

3. The presence of remaining silica as coesite, which is a high pressure transformation of silica, indicates that high thermal differential contraction stresses exist between the metal matrix and ceramic particles due to different thermal expansion coefficients.

4. Porosity increases with ceramic content, especially open porosity. From the point of view of the measured properties (porosity, hardness) the optimum amount of ceramic in these composites is about ≈ 10 vol %. For higher percentages closure of porosity could be obtained by secondary processing (repressing–resintering; hot-forging, -pressing or -rolling).

5. Hardness of the composites increases as the initial amount of ceramic is increased, from 24 BHN for sintered pure Al, up to 46 BHN for the 20 vol % specimen.

6. In the present work, relatively long sintering times were considered (24 h) in order to approach chemical equilibrium, i.e. all the silica being transformed into alumina. However, by an appropriate selection of sintering time and temperature it is possible to obtain composites with different proportions of the above mentioned phases, and thus with different mechanical properties [14].

7. Reference specimens were prepared by mixing Al powder directly with alumina particles in the same proportions (5, 10, 15 and 20 vol% Al_2O_3) and sintered under the same conditions as the Al–silica blends. In all cases the specimens thus obtained had poor bonding, even after higher sintering temperatures.

8. Liquid phase reactive sintering, in some cases, may be a simple and cheap alternative method for the obtention of PMMCs through appropriate selection of a reactive metal (Al, Ti, Mg, Ni), a ceramic powder, sintering temperature and hold time.

Acknowledgements

The present work was supported by the Proyecto Multinacional OEA-CNEA. The authors are also grateful to Ing R. A. Morando, Lic E. Vicente, Dr B. Molinas and Ing M. Markiewicz, for helpful discussions during various stages of the work. Thanks are also due to the following groups: Materiales Estructurales, Laboratorio de Microsonda Electrónica, Laboratorio de Rayos-X, Gerencia Desarrollo, CNEA.

References

1. MINORU TAYA and R. ARSENAULT, in "Metal matrix composites, thermomechanical behaviour" (Pergamon Press, Oxford, 1989).
2. I. A. IBRAHIM, F. A. MOHAMED and J. LAVERNIA, *J. Mater. Sci.* **26** (1991) 1137.
3. P. K. ROHATGI, R. ASTHANA and S. OAS, *Int. Met. Rev.* **31** (1986) 115.
4. T. DONOMOTO, N. MIURAS and K. FUNATANI, SAE Technical Paper No. 83052, Detroit, MI, 1983.
5. M. A. H. HOWES, *J. Metals* **38** (1986) 28.
6. L. CHRISTODOULOU and J. M. BRUPACHER, *Materials Edge*: **Nov** (1990) 29.
7. R. MEHRABIAN, R. G. RIEK and M. C. FLEMINGS, *Metall. Trans.* **A 5** (1974) 1899.
8. T. C. WILLIS, *Metals and Materials* **4** (1988) 485.
9. M. GUPTA, F. A. MOHAMED and E. J. LAVERNIA, *Mater. Manuf. Proc.* **5** (1990) 165.
10. C. J. QUINN and D. L. KOHLSTED, *J. Mater. Sci.* **19** (1984) 1229.
11. Y. MIYAMOTO, M. KOIZUMI and O. YAMADA, *J. Amer. Ceram. Soc.* **67** (1984) C224.
12. A. BOSE, B. MOORE, R. M. GERMAN and N. S. STOLOF, *J. Metals* **40** (1988) 14.
13. R. W. RICE, *J. Mater. Sci.* **26** (1991), 6533.
14. S. MINTZER, B. MOLINAS, M. IPOHORSKI and S. BERMUDEZ, in press.
15. O. KUBACHEWSKI and C. ALCOCK in "Metallurgical thermochemistry" (Pergamon, Oxford, 1979).
16. A. E. STANDAGE and M. S. GANI, *J. Amer. Ceram. Soc.* **50** (1967) 2, 101.
17. K. PRABRIPUTALOONG and M.R. PIGGOT, *J. Electr. Soc. Solid State* **121** (1974) 3, 430.
18. J. L. MURRAY and A. J. MCALISTER, *Bulletin of Alloy Phase Diagrams* **5** (1984) p. 1.
19. S. TAKAJO, W. A. KAYSER and G. PETZOW, *Acta Metall.* **32** (1984) 107.
20. L. COES, *Science* **118** (1953) 131.
21. W. M. GRIFFITH, YOUNG WON KIM and F. H. FROES, *ASTM Special Technical Publ.* **890** (1984) 283.
22. P. P. PRONKO, R. S. BAHATTACHARYA, J. J. KLEEK and F. H. FROES, *Metall. Trans.* **A19** (1988) 1372.

Received 8 September 1993
and accepted 22 March 1995